THE JOURNAL OF PHYSICAL CHEMISTRY C
A JOURNAL OF THE AMERICAN CHEMICAL SOCIETY



pubs.acs.org/JPCC
Article

# A Comparison of Modern Solvation Models for Oxygen Reduction at the Pt(111) Interface

Tom Demeyere and Chris-Kriton Skylaris*

Cite This: J. Phys. Chem. C 2024, 128, 19586−19600

Read Online

ACCESS | Metrics & More | Article Recommendations | Supporting Information

**ABSTRACT:** Solvation effects play an important role in the thermodynamics of catalytic reactions; however, current implicit solvation models often fail to accurately capture specific local effects, such as hydrogen bonding, limiting their ability to systematically incorporate solvation effects into quantum mechanical simulations. In this study, we investigate the Reference Interaction Site Model (RISM) and apply it to the platinum(111) interface, using the Oxygen Reduction Reaction as a case study. We compare RISM to the charge-asymmetric nonlocally determined local-electron (CANDLE) solvation model, which belongs to the class of Poisson−Boltzmann models. Our results demonstrate that RISM, with the appropriately parametrized water model can accurately describe properties of the solvated Pt(111) surface such as solvation free energies, workfunctions, and capacitances and capture subtle effects due to electrolyte concentration and explicit adsorbates. We find that including lone pairs in the water model proves to be crucial for obtaining accurate results, highlighting the importance of water nonbonding orbitals in solvation effects at the Pt(111) interface. Furthermore, RISM enables the computation of previously inaccessible properties, such as the solvent/electrolyte density near charged electrodes, providing valuable insights into the electrochemical double layer structure. Our findings suggest that RISM could serve as a computationally efficient alternative for studying electrode−electrolyte interfaces, paving the way for systematic incorporation of solvation effects into computational studies.

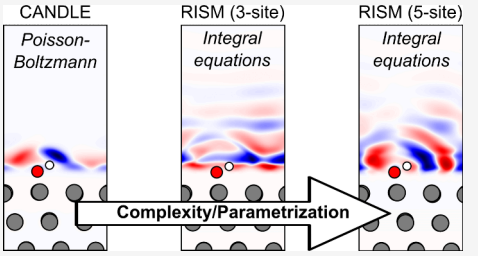




## INTRODUCTION

Several challenges must be overcome for many catalytic systems to reach commercial feasibility.[1−9] One of the direct causes is the significant overpotential at the catalyst surface due to the complex reaction mechanisms involved.[10−13] To design the next generation of catalysts, it is crucial to obtain accurate microscopic properties such as free energies of adsorption, free energies of solvation, activation energies and surface charges.[14,15] These properties undergo important variations due to operational conditions, including the presence of solvent and electrolytes. Possible insights on these variations using experimental techniques are restricted by both technical and physical limitations, and often computational techniques are required.[16−18] Analogously, there are important limitations in computational modeling preventing a fully accurate description of the electrochemical interface. In order to obtain thermally integrated properties for electrochemical systems, it is necessary to sample the phase space at constant potential. Explicit sampling of the solvent and electrolytes is required to accurately describe the interface but is still computationally unfeasible. Furthermore, because the Fermi energy is a bulk property, simulations involving finite-sized electrodes will require larger simulation cells to minimize fluctuations of this quantity. To address this problem, the solvent is often replaced by a dielectric medium that aims to reproduce electrostatic features of solvation. In the same fashion, electrolytes are often replaced by a continuous charge density using Poisson−Boltzmann models. In combination, the potential of the simulation cell can be fixed using recent approaches such as Grand-Canonical DFT, allowing the total number of electrons to change while keeping the Fermi energy constant.[19−25] Alternative approaches include combining explicit water and implicit solvation[26−28] along with exploring various charge screening methods.[29,30] For instance, capacitor-based approaches, which rely on simple but effective thermodynamic assumptions, have been successful in accurately describing both reaction and activation energies of the Oxygen Reduction Reaction (ORR).[31−35] In these models, the double layer is formed by one or more water layers with added or removed protons. However, this technique requires a large unit-cell and still lacks proper solvent and electrolytes sampling.

In an attempt to tackle the various challenges previously cited, an important amount of work has been dedicated to the development of implicit solvation models.[36−51] While these models have proved helpful for small, isolated solutes, their

Received: July 22, 2024
Revised: October 12, 2024
Accepted: October 28, 2024
Published: November 12, 2024

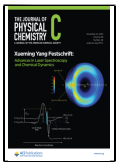





https://doi.org/10.1021/acs.jpcc.4c04924
J. Phys. Chem. C 2024, 128, 19586−19600

accuracy is often assumed to be transferable to the electrochemical interface without extensive justifications. Additional terms such as dispersion and repulsion corrections or entropic considerations are often heavily parametrized for specific molecular data sets. For this reason, their usefulness for different environments, such as electrochemical interfaces, is unknown. Additional issues arise when considering electrochemical systems such as the lack of quadrupole interactions which can considerably affect energy levels.[52] Conventional Poisson−Boltzmann models depict electrolytes as continuous charge-density with exponential decay, therefore, ignoring angular and orientation contributions. This leads to a simplified model of the double layer with important shortcomings when considering effects arising far from the Potential of Zero Charge (PZC) or when the size of the electrolytes becomes significant.

More advanced solvation models such as the Reference Site Interaction Model (RISM), or classical DFT[51] might provide answers to these problems. In this study, we use RISM[53,54] implemented in the Quantum Espresso software.[55,56] The implementation of RISM within a DFT framework has been used to study various systems and capture properties that are not available using conventional implicit models.[57−59] RISM is often called a structured implicit solvation model, since it is able to capture thermodynamically integrated structural information about the solvent and electrolytes.

Practically, the solvent and electrolytes are represented by sites with physical properties such as charges, positions, and a set of Lennard-Jones parameters. Thermodynamic properties are then integrated from the computed correlation functions.[60] For more information, the reader is redirected to the original paper from Kovalenko and Hirata.[53] The RISM model can be coupled with the Effective Screening Medium (ESM)[61,62] technique which makes use of Green's functions to impose various boundary conditions on the DFT unit cell. By imposing open boundary conditions on one of the spatial dimensions, ESM is able to yield a nonrepeated slab approach. Thus, within ESM-RISM, the electrostatic potential in the solvent region can be defined as an origin for energy levels. Additionally, the charge in the unit cell is screened by the RISM solvation model at the interface. The ESM-RISM scheme can model an isolated surface accounting for effects of solvation, pH, temperature and possibly the electrode potential along with structural information about the solvent.[63]

This study focuses on computing relevant properties of the Pt(111) interface such as solvation energies, workfunctions, capacitances, and solvent distributions. We also investigated the behavior of our models for catalytic reactions by using the ORR as a case study. First, computational parameters used for ESM-RISM will be explained, which includes parameters for both the DFT solute atoms and the solvent/electrolyte RISM sites. Two water parametrizations will be used for the RISM model; the 3-site SPC model[64] and the 5-site TIP5P model,[65] both of which are well-known water models. The latter additionally includes negatively charged sites to account for the lone-pairs. The same set of calculations will also be carried out using the Charge-Asymmetric Nonlocally Determined Local-Electric (CANDLE) solvation model.[66] The model is a more computationally feasible version of the nonlocal Spherically Averaged Liquid Susceptibility Ansatz (SaLSA) model.[51] CANDLE stands out by its ability to treat both anions and cations accurately without the need for specific fittings.[66] This is explained by the nonlocal dependence of the cavity on the solute electric field, which enables the model to capture charge asymmetry. Additionally, this model belongs to the large ensemble of available and well-understood cavity-based implicit solvation models. For these reasons, it was chosen as a basis for comparison with RISM in this study, aiming to compare RISM with a model whose behavior is better understood.

We then present our results, including free energies of solvation and adsorption with both RISM water models and CANDLE. At the same time, we include comparison with the static-bilayer approximation, a widely used method where only the first layer of explicit water is considered. We further discuss these results by plotting the 2D averaged solvent charge at the interface in an attempt to explain the disparities between our models. In a second part we explain how we compute workfunctions for solvated systems and compare them between the models. We then perform calculations outside the PZC at different surface charge densities. For each of these calculations, we plot the RISM density distributions for hydrogen and oxygen water sites and show that the model correctly predicts the H-up to H-down flip around the PZC. We continue to discuss the implications of our findings and the need for a comparison with properly sampled Ab-Initio Molecular Dynamics (AIMD) simulations. Using the previous calculations, we are also able to compute differential capacitance curves and compare them to expected behavior. Finally, we quickly discuss computational stability and convergence along with challenges that are yet to be tackled.

## METHODS AND COMPUTATIONAL DETAILS

**ESM-RISM.** ESM-RISM calculations have been carried out using the Quantum Espresso software[55,56] (7.2). We used the pseudopotentials from the SSSP efficiency library,[67−69] that is pslibrary 0.3.1 for O (6 valence electrons: $2s^2 2p^4$), pslibrary 1.0.0 for H (1 valence electron: $1s^1$), but deviated from the recommended GBRV 1.4 library for Pt, where instead the SG15 norm-conserving pseudopotential[70] (18 valence electrons: $5s^2\ 5p^6\ 6s^2\ 5d^8$) was used. For RISM calculations, switching to this pseudopotential reduced the initial charge sloshing behavior and led to a much smoother convergence. The associated energy cutoff was set to 815 eV. The Pt(111) surface is represented by a $3 \times 3$ slab and a $\sqrt{3} \times \sqrt{3}$ R45 slab both consisting of five layers for 1/9 ML and 1/3 ML coverage calculations, respectively. The Brillouin zone is sampled with a Monkhorst−Pack grid[71] of $4 \times 4 \times 1$ and $8 \times 8 \times 1$ for the largest and smallest cells, respectively. We used the RPBE functional[72] coupled with the D3 correction[73] as it showed improved energetics for oxygenated and hydrogenated systems on Pt(111).[74] Geometry optimizations were done keeping the two bottom layers held fixed; the force criterion was set to be less than $10^{-3}$ Ry/Bohr, along with an energy criterion of $10^{-5}$ Ry. Solvent and electrolyte concentrations are directly specified in the Quantum Espresso input file, along with their MOL files containing site parameters. Two sets of calculations will be performed at concentrations of 0.1 and 1.0 M. For more information about the ESM-RISM theory, the reader is redirected to the paper of Nishihara and Otani.[60]

Within the RISM framework, interactions between solvent sites and the solute atoms are described classically by using a Lennard-Jones potential. As such, solvent and electrolyte sites must have well-defined properties such as atomic positions, charge, and Lennard-Jones parameters. These parameters must



https://doi.org/10.1021/acs.jpcc.4c04924
J. Phys. Chem. C 2024, 128, 19586−19600

be chosen carefully in order to reproduce the desired properties. RISM parameters used throughout the study for solute (DFT) atoms are summarized in Table 1 and are the same for both water models. The detailed set of parameters for RISM sites in the water models are described in multiple studies,[75,76] along with the electrolyte parameters for $H_3O^+$[77] and $Cl^-$.[78]

**Table 1. RISM Lennard-Jones Parameters for DFT Solute Atoms Used with Both RISM (SPC) and RISM (TIP5P) Water Models from a Study of Haruyama et al.[75]**

| | $\epsilon$ (kcal/mol) | $\sigma$ (Å) |
|---|---|---|
| Pt | 1.660 | 2.65 |
| O | 0.160 | 3.12 |
| H | 0.046 | 1.00 |

In ESM-RISM the solvent is confined only in one part of the cell, as shown in Figure 1, this is done by imposing different boundary conditions on each side of the cell. The solvent starting position can be specified using a Quantum Espresso keyword (*laue_starting_right*). This choice can be guided by an energy minimization scheme[63] or chosen arbitrarily.[58] Because the first approach might give unphysical situations where the solvent starts far away from the metal, we place it between the two-right side outermost layers of the slab as done in previous studies.[58]

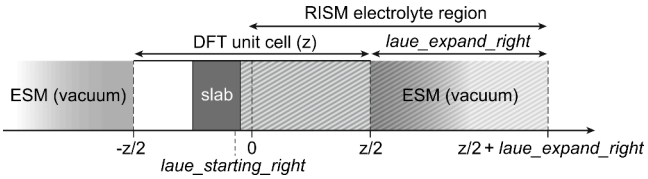


**Figure 1.** Schematic of the DFT unit cell setup with ESM-RISM. The DFT region along the direction perpendicular to the surface is changed from $(0, z)$ to $(-z/2, z/2)$. The total RISM region where the correlation functions are calculated starts at *laue_starting_right* and ends at $z/2$ + *laue_expand_right*. Adapted from ref 58. Available under a CC BY 4.0 license. Copyright 2021 Tesch et al.

Similarly, the expansion region for RISM correlation functions can be specified using another Quantum Espresso keyword (*laue_expand_right*) and has been chosen to be equal to 40 Å. The total size of the unit cell along the perpendicular direction is equal to 60 Å. For both models, a solvent temperature of 298.15 K was chosen, and the solvent energy cutoff was taken as four times the wave function cutoff; 3260 eV. The 3D-RISM convergence criteria for both models is set to $10^{-6}$ Ry.

**CANDLE.** To perform the CANDLE calculations the JDFTx software[79] was used with the same starting geometries. After testing the various parameters for convergence and to ensure maximum compatibility throughout the study, general DFT parameters e.g. energy cutoffs, k-point grid, and spin-polarization, are chosen similar to the one used for Quantum Espresso. The Brillouin zone is sampled with a Monkhorst–Pack grid[71] of $4 \times 4 \times 1$ and $8 \times 8 \times 1$ for the different slab sizes. Calculations are spin-polarized, and energy cutoffs are chosen as 30 and 240 Ha for wave functions and charge density, respectively. The occupancies are smeared using the cold smearing method with a smearing parameter of 0.01 Ha. Geometry optimizations were done keeping the two bottom layers held fixed, the force and energy criteria were set to be less than $5.0 \times 10^{-4}$ Ha/Bohr, and $1.0 \times 10^{-6}$ Ha, respectively. A slab type Coulomb cutoff is applied, and to make sure that the charge density is confined within half of the cell in the $z$ direction, $c$ has been chosen to be equal to 75.58 bohr for all geometries. Because calculations with CANDLE generally display much better convergence behavior, we fully use the SSSP recommended pseudopotentials, that is, GBRV 1.4 (16 valence electrons: $5p^6 5d^{10}$) for Pt, pslibrary 1.0.0 for H (1 valence electron: $1s^1$) and pslibrary 0.3.1 for O (6 valence electrons: $2s^2 2p^4$). For CANDLE solvation specific parameters, we use the default parametrization for cavity and electrolytes. To ensure basic commensurability between both software packages, formation energies were computed in vacuum, and the maximum difference was found to be less than 0.05 eV for similar systems.

## RESULTS

**Formation Energies.** All Gibbs free energies are computed at 298.15 K using eq 1 where the Zero Point Energy (ZPE) $E_{ZPE}$, thermal energy $E_{vib}^{298.15K}$, and entropy $S_{vib}^{298.15K}$ are calculated within the harmonic approximation. The required phonon calculations have been performed on a simpler Pt(111) slab consisting of 12 atoms ($\sqrt{3} \times \sqrt{3} \times 4$) for each adsorbate. The thermodynamic properties were obtained by integration of the phonon density of states. More details are available in the Supporting Information.

$$G_{ads}^{298.15K} = E_{DFT} + E_{ZPE} + E_{vib}^{298.15K} - TS_{vib}^{298.15K} \quad (1)$$

Throughout the study we apply the Computational Hydrogen Electrode[10] (CHE) which assumes the equilibrium of eq 2. This avoids the need to calculate the chemical

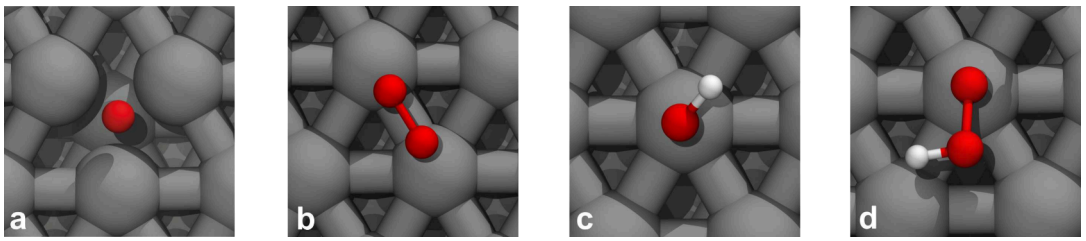


**Figure 2.** Adsorbates under study on the Pt(111) electrode. Sites have been selected based on their known stability from the literature; (a) fcc for O*, (b) bridge for $O_2^*$, (c) ontop for OH*, and (d) top-bridge for OOH*. For O*, $O_2^*$ and OH* all calculations are done on the $3 \times 3$ ($\theta$ = 1/9 ML) and $\sqrt{3} \times \sqrt{3}$ R45 ($\theta$ = 1/3 ML) surfaces. OOH* is only investigated at $\theta$ = 1/9 ML.



https://doi.org/10.1021/acs.jpcc.4c04924
J. Phys. Chem. C 2024, 128, 19586−19600

potential of the proton in a solvent and provides a simple but efficient link to the electrode potential.

$$H^{+}_{(aq)} + e^{-}_{(vac)} = \frac{1}{2}H_{2(g)} \quad (2)$$

For calculations in vacuum and using the solvent models, we consider the reactions given in eq 3 where the O, OH, OOH, and $O_2$ intermediates are adsorbed on the sites * of the clean Pt(111) surface. Sites are chosen based on their stability from the literature[80,81] and shown in Figure 2.

$$2H_2O_{(l)} + * \rightarrow O_2^* + 2H_{2(g)}$$
$$2H_2O_{(l)} + * \rightarrow OOH^* + \frac{3}{2}H_{2(g)}$$
$$H_2O_{(l)} + * \rightarrow O^* + H_{2(g)}$$
$$H_2O_{(l)} + * \rightarrow OH^* + \frac{1}{2}H_{2(g)} \quad (3)$$

For calculations including a static water bilayer, it is assumed that adsorbates bind to the same sites and replace a water molecule in the bilayer, as described in the reactions given in eq 4.

$$6H_2O^* + H_2O_{(l)} \rightarrow 5H_2O^* + O_2^* + 2H_{2(g)}$$
$$6H_2O^* \rightarrow 5H_2O^* + O^* + H_{2(g)}$$
$$6H_2O^* \rightarrow 5H_2O^* + OH^* + \frac{1}{2}H_{2(g)}$$
$$6H_2O^* + H_2O_{(l)} \rightarrow 5H_2O^* + OOH^* + \frac{3}{2}H_{2(g)} \quad (4)$$

Implicit solvation models have been widely used in the literature to study the thermodynamics of the ORR.[82−84] However, solvation energies computed with various implicit models can differ as much as 0.8 eV.[85] Such energy differences can lead to drastically different conclusions about the reaction's thermodynamic landscape. These discrepancies are likely due to variations in implicit solvation parameters, particularly the cavity size, where small differences can result in large solvation energy variations.[85] These significant differences can also be attributed to the various conventions used to calculate thermodynamic properties when solvation is considered. Using the clean surface in vacuum as a reference typically leads to increased stabilization[82] of adsorbates since the solvation energy of the clean surface tends to be negative. In this paper we use the solvated surface convention, i.e., the water covered surface is used as a reference (* in eq 3).

Figure 3 presents the Gibbs formation energies ($G_{ads}^{298.15K}$) computed using eq 3 and eq 4 for each ORR intermediate. Throughout the study, we use the terms stabilization and destabilization to describe the solvation effects with respect to vacuum energies. Non-hydrogenated species (O* and $O_2^*$) are unaffected by the CANDLE model, while both RISM (SPC) and RISM (TIP5P) destabilize these species by (0.11, 0.34) and (0.08, 0.25) eV, respectively. Hydrogenated species (OH* and OOH*) both experience small stabilization by the CANDLE model, while the RISM (SPC) and RISM (TIP5P) models predict slight destabilization. Our results are consistent with previous implicit solvation studies, which typically show a significant underestimation of the stabilization for hydrogenated species compared to the explicit static-bilayer.

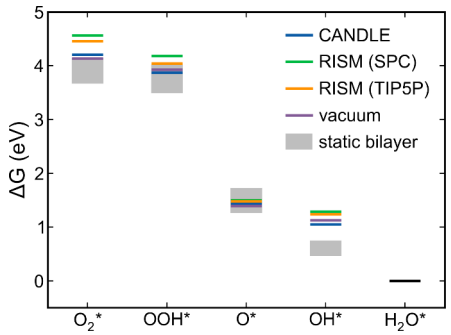


**Figure 3.** Free energy diagram for all different models under study, CANDLE, RISM (SPC), and RISM (TIP5P). All energies are taken from simulations done at an electrolyte concentration of 1 M and coverage of 1/9 ML. Static bilayer calculations are represented as ranges as explained in the text. For solvated calculations the water covered surface is used as a reference and is set to 0 eV.

Numerous studies have employed explicit water techniques to investigate the ORR.[28,86−91] Similarly to implicit solvation studies, they often display significant disparities, particularly when different functionals and dispersion corrections are used.[92] Furthermore, using different water orientations, H-down or H-up, can lead to inconsistent results. Finally, these disparities can also arise due to a different treatment of the entropy for adsorbed water. Calculations in vacuum and using implicit solvent models often assume that the water reference is taken from a gaseous or liquid reservoir where translation, rotation, and vibration entropy terms are included, and taken from thermodynamic tables. For explicit water studies, instead, this reference is frequently a water molecule removed from the electrode ($H_2O^*$), and only vibrational degrees of freedom are used. This latter contribution $S_{vib}$ is typically much smaller (0.06 eV) than the full standard gas entropy $S$ (0.67 eV) which leads to a considerable overestimation of the binding strength for explicit calculations.

Estimating the exact entropy of water molecules on Pt(111) is challenging. A lower bound can be obtained by considering the standard entropy of solid water (ice) which is estimated to be ≈0.12 eV.[93,94] In this scenario, water molecules at the interface are ice-like and are not free to move. Considering that previous experimental and theoretical studies have shown that water retains some mobility at the Pt(111) interface,[95,96] this view will underestimate the entropy of water at the interface. The opposite argument would be to consider that water molecules are free to move and rotate, leading to the same entropy as that in the liquid phase, likely overestimating the entropy. A more accurate approach might be to make use of the work from Campbell and Sellers,[97] who studied the entropy of adsorbate molecules on various surfaces and found a linear dependence between the entropy of the adsorbate and its gaseous equivalent. Using their formula, we find a value of 0.38 eV, right between the two extremes. However, the authors specifically mention that their approximation holds for adsorbates with attractive lateral interactions. This assumption does hold for water, but given the complex interactions with other water molecules due to hydrogen networks, further investigation is needed to confirm the validity of this approximation for the water-Pt(111) interface.



https://doi.org/10.1021/acs.jpcc.4c04924
J. Phys. Chem. C 2024, 128, 19586−19600

For the purpose of this study, we show the static bilayer results as a range to account for these uncertainties. Additionally, in this range, we include the energy difference due to the orientation of water. As a result, the lowest energy is taken as the most stable configuration between the H-down and H-up calculations, and the entropy is taken as 0.38 eV. Oppositely, the highest energy is taken as the least stable configuration, and the entropy is taken as 0.67 eV.

Despite these variations, there is a consensus that the formation of a hydrogen bonding network leads to a substantial stabilization of hydrogenated species,[90] more pronounced for OH*. Our results for the static bilayer, as shown in Figure 3 are consistent with these expectations. We find that OH* is stabilized by at least −0.38 eV, and at most −0.67 eV, which is comparable to the values reported by Heenen et al.[28] using AIMD (−0.58 eV), He et al.[98] (−0.57 eV), and Di Liberto and Giordano[99] (−0.71 eV). For OOH*, results are more contrasted, with the adsorbate either stabilized by up to −0.44 eV, but possibly destabilized by 0.09 eV. Such destabilization have not been reported in the literature, with reported values of −0.49 eV[98] and −0.25/-0.79 eV.[90] Our results indicate that O* is not significantly affected by solvation, which we attribute to its proximity to the surface and the absence of hydrogen bonds. Finally, we find that $O_2^*$ can either be unaffected or stabilized up to −0.47 eV. This latter finding is subject to ongoing discussion, as it is often thought that $O_2^*$ is unaffected by solvation. Nevertheless, a study by Liu et al.[35] has demonstrated that $O_2^*$ can indeed be stabilized by static bilayer. The discrepancies within the literature values for OOH* and $O_2^*$ suggest that subtle changes in water orientation can have a significant impact on the solvation stabilization of larger intermediates. To adequately capture these effects and improve our understanding of the solvation environment for ORR intermediates, more extensive sampling techniques will be required in future studies.

The systematic destabilization of adsorbate predicted by both RISM models can be understood by examining Table 2 where the clean Pt(111) surface has a notably strong solvation energy, but all solvation stabilization weakens when adsorbates are added. For all our models, the solvation energy is computed by taking the difference in energy between the system in solvent and in vacuum.

**Table 2. Absolute Solvation Free Energies (eV) Calculated with the Different Solvation Models for Each Adsorbate at Different Electrolyte Concentrations**[a]

| | CANDLE | | RISM (SPC) | | RISM (TIP5P) | |
|---|---|---|---|---|---|---|
| | 1.0 M | 0.1 M | 1.0 M | 0.1 M | 1.0 M | 0.1 M |
| clean 3 × 3 | −0.33 | −0.33 | 0.83 | 0.56 | −0.37 | −0.62 |
| clean $\sqrt{3} \times \sqrt{3}$ R45 | −0.11 | −0.11 | 0.28 | 0.19 | −0.12 | −0.20 |
| O (1/3) | −0.11 | −0.11 | 0.39 | 0.28 | −0.03 | −0.13 |
| O (1/9) | −0.33 | −0.33 | 0.94 | 0.65 | −0.29 | −0.55 |
| $O_2$ (1/3) | −0.08 | −0.08 | 0.7 | 0.54 | 0.19 | 0.04 |
| $O_2$ (1/9) | −0.30 | −0.30 | 1.17 | 0.84 | −0.12 | −0.41 |
| OH (1/3) | −0.15 | −0.15 | 0.46 | 0.33 | 0.01 | −0.11 |
| OH (1/9) | −0.40 | −0.40 | 0.94 | 0.64 | −0.34 | −0.61 |
| OOH (1/9) | −0.39 | −0.39 | 1.09 | 0.75 | −0.26 | −0.57 |

[a]Solvation energies obtained using ESM-RISM depend on the `laue_starting_right` parameter.

$$\Delta G_{solv} = G_{solvent}(\boldsymbol{R}') - G_{vacuum}(\boldsymbol{R}) \quad (5)$$

where $G_{solvent}$ and $G_{vacuum}$ are the Gibbs free energies of the system in solvent and vacuum, respectively. $\boldsymbol{R}'$ and $\boldsymbol{R}$ are the relaxed atomic positions for the solvated system and the vacuum one. For RISM models, the total solvation energy can be further decomposed between two contributions, the excess chemical potential of solvation $\mu_{ex}$, and the residual contribution $G_{res}$. The latter coming from changes either in the geometry or in the electronic structure due to solvation.

$$\Delta G_{solv} = \mu_{ex} + G_{res} \quad (6)$$

The first contribution is directly computed from the RISM correlation functions.[60] We find a clear domination of this term in all solvation energies reported in Table 2, with the residual often accounting only for less than 5% of the total solvation energy. Interestingly, the excess term should account for both stabilizing and destabilizing effects involved in solvation such as the energy cost to replace water molecules. Lee and Schmidt[100] recently pointed out that implicit solvent calculations should be corrected to account for the latter. This cost is accounted for in our bilayer calculations by explicitly removing a water molecule. For the RISM models, we argue that this cost is directly included in the excess term. This is supported by the fact that RISM needs to compute the total number of sites and therefore the total number of solvent molecules for a given simulation cell volume. Since the excess term is directly computed as a summation over sites,[60] placing explicit molecules should directly impact the excess term. As an example, for the clean Pt(111) $\sqrt{3} \times \sqrt{3}$ R45 slab a total of 50.21 water molecules are estimated by RISM for the entire simulation cell. This number decreases to 48.95 (−1.26 water molecules) if OH* is added on the surface.

The free energy of solvation obtained using the RISM (TIP5P) model for the clean Pt(111) electrode is in good agreement with a recent estimate by Bramley et al.,[94] who employed additional thermodynamic assumptions to compute an estimate of the entropy of solvation. The authors provided a range for the solvation free energy of the Pt(111) interface to be between −0.05 and −0.07 eV/(Pt atom). The TIP5P model gives values of −0.04 and −0.07 eV/(Pt atom) for electrolyte concentrations of 1 and 0.1 M, respectively. CANDLE also predicts reasonable solvation energies for the Pt(111) surface, giving for both electrolyte concentrations a solvation energy of −0.04 eV/(Pt atom). This agreement suggests that both the RISM (TIP5P) and CANDLE models provide a reasonable description of the solvation environment at the electrode−electrolyte interface. In contrast, the RISM (SPC) model yields a significantly higher solvation energy, which has been previously shown to be inaccurate.[101] For the RISM (TIP5P) model, a reasonable description of the solvation energy for the clean Pt(111) surface indicates that the model should correctly describe the removal of water molecules from the interface.

RISM models predict a well-structured, symmetric solvation profile on the clean slab, which can be seen through the solvent charge distribution plots in Figure 4. However, when adsorbates are added, the profiles seem to be highly destabilized, resulting in more disordered solvation structures (Supporting Information). This apparent symmetric solvation profile on the clean surface might be generated due to the symmetry of the slab itself and, as a result, is highly disrupted when an adsorbate is added. The disruption possibly has an


https://doi.org/10.1021/acs.jpcc.4c04924
J. Phys. Chem. C 2024, 128, 19586−19600

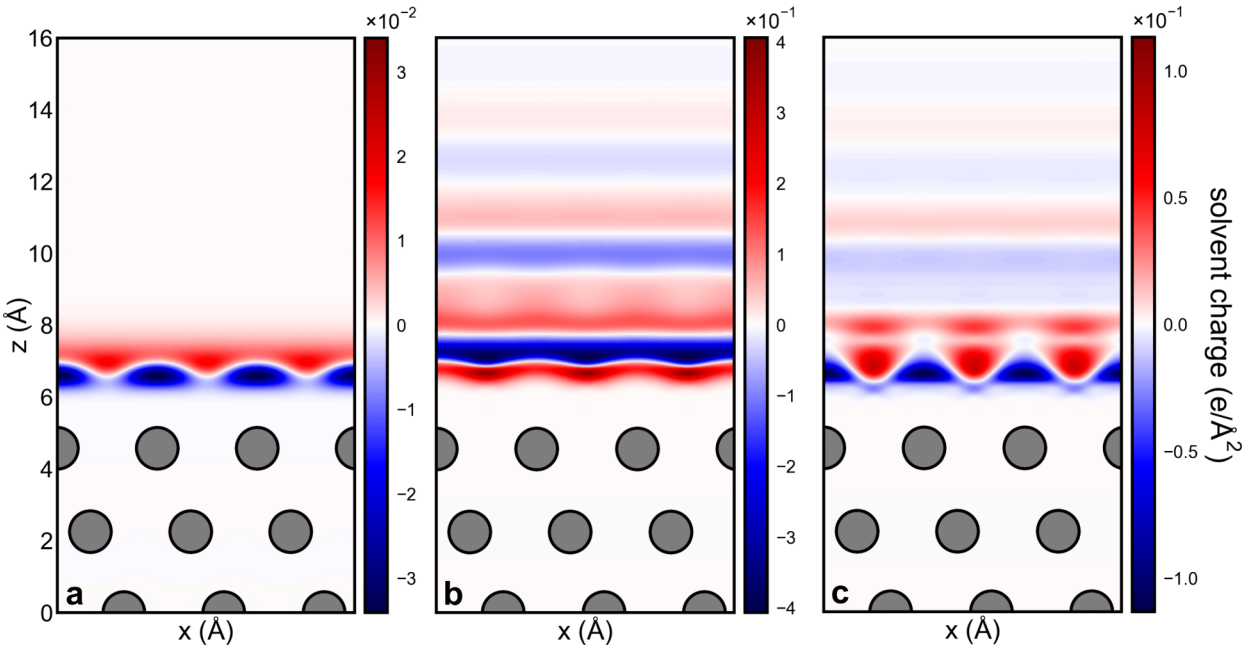


**Figure 4.** 2D planar averaged solvent charge polarization along the *y* direction for the different solvation models (a) CANDLE, (b) RISM (SPC), (c) RISM (TIP5P) for the clean 3 × 3 Pt(111) surface at 1.0 M. Gray spheres are platinum atoms.

important impact on the excess chemical potential term $\mu_{ex}$, leading to an artificial destabilization.

Both of the RISM models show significant solvation energy variations when changing the electrolyte concentrations. The main contribution difference comes from the excess chemical potential term $\mu_{ex}$ calculated by RISM. This suggests that RISM predicts significant destabilization of the water structure at the interface for high electrolyte concentrations. However, we were unable to find any meaningful comparisons in the experimental literature to validate this observation. Since the CANDLE model does not exhibit such differences, the effect might stem from solvent/electrolyte interactions, which are included in the correlation function of RISM. In contrast, traditional Poisson−Boltzmann models account for electrolyte−electrolyte interactions only through their mean electrostatic potential. Similarly, the interaction of the solvent cavity with electrolytes is accounted for only indirectly through the DFT electronic density. In the non-size-modified framework, Poisson−Boltzmann ions do not occupy space, which may lead to an underestimation of the impact of electrolyte concentration depending on the parametrization.

Although the plots presented in Figure 4 have limited quantitative meaning, they provide valuable insights into the interfacial description given by each model. CANDLE, being a linearized Poisson−Boltzmann model, results in a strong aggregation of point charges limited to the vicinity of the metal, as shown in Figure 4a. In contrast, both RISM models exhibit a more diffuse and complex double layer in Figure 4b (SPC) and Figure 4c (TIP5P).

Interestingly, both CANDLE and the RISM (TIP5P) models show similar trends close to the interface with the formation of negatively charged cavities directly above the platinum atoms. The spaces between these cavities serve as wells for positive charge accumulation. On the other hand, the SPC model depicts the interface with a positively charged first layer. This observation can be explained by examining the 2D averaged density plots for both models which are available in the Supporting Information. These plots reveal that for the RISM (SPC) model, the hydrogen sites are located slightly beneath the oxygen sites. This arrangement, without the flexibility of the 5-site model results in a more simplistic representation of the interfacial structure. In contrast, the RISM (TIP5P) model presents a complex picture of the charge distribution at the platinum-water interface (Figure 4c), with a strong spatial dependence along the direction parallel to the surface. The 2D averaged density plots for the RISM (TIP5P) model show that the oxygen sites are not at maximum density directly above the platinum atoms (ontop sites) but rather between them (hollow sites). The hydrogen sites are positioned broadly with minima on top of platinum atoms, while the additional negatively charged lone-pair sites are mainly located directly above the platinum atoms, contributing to the formation of negatively charged cavities. The average positions of oxygen sites, not directly above platinum atoms, might be an issue of the current RISM (TIP5P) model. This can be explained by considering the current charge parametrization where lone-pair sites are entirely responsible for modeling the negative charges, while the oxygen site is assumed neutral.

**Workfunctions and Potentials of Zero Charge.** Workfunctions play a crucial role in electrochemistry due to their direct connection with electrode potentials.[102] Computing workfunctions in a vacuum is relatively straightforward, as it is calculated by taking the difference between the Fermi energy of the electrode and the electrostatic potential in a vacuum close to the surface. However, determining solvated workfunctions requires additional considerations.[103] In this section, we first explain the methodology used to compute the PZC for each model and then compare the obtained workfunctions with those reported in the literature. The absolute value of the Standard Hydrogen Electrode (SHE) can be directly computed by considering the equilibrium of reaction 7.

$$H_3O^+_{(l)} + e^-_{(vac)} = H_2O_{(l)} + \frac{1}{2}H_{2(g)} \quad (7)$$



https://doi.org/10.1021/acs.jpcc.4c04924
J. Phys. Chem. C 2024, 128, 19586−19600

The experimentally determined absolute value of the SHE is 4.44 V,[104] computed using a reference for the energy levels outside the water/vacuum interface. Hence, we need to account for the energy required for the proton to cross the water/vacuum interface. This additional term $\chi_S$ accounts for this surface dipole: $\alpha_{H_3O^+} = \mu_{H_3O^+} + \chi_S$ and leads to eq 8.

$$U_{SHE}^{\circ}(\text{abs}) = \frac{\mu_{H_3O^+} - \mu_{H_2O} - 1/2\mu_{H_2}}{e_0} + \chi_S \tag{8}$$

The chemical potentials $\mu_{H_3O^+}$, $\mu_{H_2O}$, and $\mu_{H_2}$ were determined through calculations conducted either in vacuum or in solvent. As a first approximation, ZPEs are calculated in vacuum using the Phonopy package.[105,106] Entropy contributions are taken from the NIST-JANAF thermodynamic tables in their corresponding states.[107] The values obtained using this approach are 5.58 V for the RISM (SPC) model and 4.98 V for the RISM (TIP5P) model. The accuracy of these values is highly dependent on the quality of the solvation energies. Since the RISM (TIP5P) model has been parametrized to replicate solvation energies, it is expected to provide a more accurate prediction of the absolute value of the SHE. The solvation energies given by RISM (TIP5P) are −89 kcal/mol for $H_3O^+$ and −3.20 kcal/mol for $H_2O$, compared to −71 kcal/mol for $H_3O^+$ and −1.38 kcal/mol for water given by the RISM (SPC) model. Solvation energies of the former are closer to the estimated experimental data of −103.45 kcal/mol for the hydronium ion[108] and −6.3 kcal/mol for water.[109] These findings suggest that the RISM (TIP5P) model provides a more accurate description of the solvation environment and, consequently, a more reliable estimate of the SHE absolute value compared with the SPC model. The computed absolute levels for the SHE using both of our models are then compared to the energy required to remove an electron from the electrode to the vacuum just outside the water/vacuum interface i.e., the solvated workfunction $W_{M|S}$

$$U_{M|S}(\text{abs}) \equiv \frac{W_{M|S}}{e_0} = \Delta_M^S\phi - \frac{\mu_M}{e_0} + \chi_S \tag{9}$$

In this equation, $\mu_M$ is the Fermi energy of the metal and $\Delta_M^S\phi = \phi_M - \phi_S$ represents the inner potential difference between the metal and the solvent. The involved electrochemical quantities are all shown in Figure 5 where the outer (Volta) potential $\psi_\alpha$ is defined as the work required to bring a unit point charge from far away to just outside the surface of the phase $\alpha$. The inner (Galvani) potential $\phi_\alpha$ represents the work needed to bring the point charge from far away to a point inside phase $\alpha$. The difference between these two potentials is the surface potential $\chi_\alpha$ that arises from the inhomogeneous charge distribution at the phase interface.

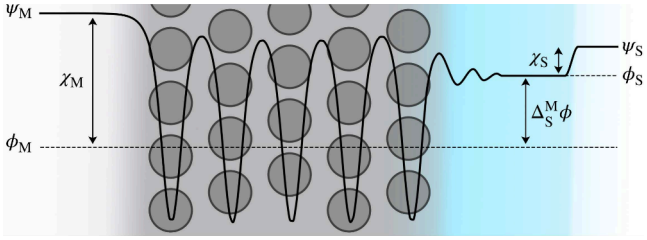


**Figure 5.** Schematic of the involved electrochemical energy levels at the metal−water interface. For a given phase $\alpha$, $\phi_\alpha$ is the inner (Galvanic) potential, $\psi_\alpha$ is the outer (Volta) potential and $\chi_\alpha$ is the surface potential.

Both eqs 8 and 9 require the value of surface potential $\chi_S$. However, computing this quantity is not a trivial task, even when using more advanced techniques such as AIMD.[110] We bypass the need for $\chi_S$ by noting that this term cancels out when subtracting the two equations. This approach is often called the Computational Standard Hydrogen Electrode (CSHE) method, where the absolute level is directly computed from thermodynamic arguments. The method tacitly assume that the calculated surface potential ($\chi_S^{calc}$) and the experimentally measured surface potential ($\chi_S^{exp}$) are equal, that way, the influence of $\chi_S$ is removed. This is in contrast with the Wave Function (WF) method, where the workfunction is calculated explicitly, often by taking the energy level of the vacuum above the water film, which is not possible in our simulations. This vacuum level is assumed to be aligned with the absolute vacuum level, and the value of such workfunction is directly compared to the accepted absolute value of the SHE (4.44 V). In this case, the surface potential contribution is implicit and is assumed different from experimental values. As a result, the workfunction between both methods mainly differs by a constant shift.[111] Interestingly, important discrepancies have been reported between the experimental and calculated values of the surface potential $\chi_S$ of water. Multiple experimental studies reported low positive values (≈ 0.13 V),[103,112,113] while calculated values are often negative and large (−0.54 V)[114] which Fawcett[103] mentioned as unphysical. This is the case for the RISM (TIP5P) model which predicts a surface potential in agreement with this value of −0.54 V. In this work, we argue that only the difference of $U^{\circ}_{SHE}$ and $U_{M|S}$(abs) carry physical meaning:

$$U_{M|S}(\text{SHE}) = U_{M|S}(\text{abs}) - U_{SHE}^{\circ}(\text{abs}) \tag{10}$$

The absolute values of the quantities involved in eq 10 are directly related to RISM parameters and referenced to the inner potential of the solvent and as a result are not comparable to experiment. Additionally, within the ESM-RISM approach, the boundary conditions are chosen such that $\phi_S = 0$ in the bulk solvent. Consequently, eq 9 further simplifies:

$$U_{M|S}(\text{abs}) = -\underbrace{\left(\frac{\mu_M}{e_0} - \phi_M\right)}_{\tilde{\mu}_M = E_F} + \chi_S = -E_F + \chi_S \tag{11}$$

where $E_F$ is the Fermi energy directly obtained from the DFT calculations. Consequently, eq 10 can be calculated simply by taking the difference between this quantity and the value obtained above for $U_{SHE}^{\circ}$(abs).

$$U_{M|S}(\text{SHE}) = -E_F - \frac{\mu_{H_3O^+} - \mu_{H_2O} - 1/2\mu_{H_2}}{e_0} \tag{12}$$

For the CANDLE model, the complications associated with computing the absolute value of the SHE $U_{SHE}^{\circ}$(abs) have been avoided by comparing the experimental PZC values against calculated ones for various metal surfaces.[66] The absolute value of the SHE was then determined by performing a linear fitting.[115,116] Here, we use the value of 4.66 V obtained from previous works.



https://doi.org/10.1021/acs.jpcc.4c04924
J. Phys. Chem. C 2024, 128, 19586−19600

Table 3. Workfunctions for Each Solvation Model (eV), Vacuum Results Are Also Included

| | CANDLE | | RISM (SPC) | | RISM (TIP5P) | | | |
|---|---|---|---|---|---|---|---|---|
| | 1.0 M | 0.1 M | 1.0 M | 0.1 M | 1.0 M | 0.1 M | vacuum | literature |
| clean | 5.04 | 5.04 | 4.53 | 4.51 | 4.81 | 4.97 | 5.53 | 4.86,[a] 4.96,[b] 5.51,[c] 4.80,[e] 4.65,[f] 5.00,[g] 4.83,[h] 4.7[i] |
| O (1/3) | 5.22 | 5.22 | 4.73 | 4.74 | 4.96 | 5.00 | 5.69 | 5.76[k] |
| O (1/9) | 5.07 | 5.08 | 4.55 | 4.56 | 4.87 | 5.00 | 5.58 | 5.61[j] |
| $O_2$ (1/3) | 5.39 | 5.39 | 5.25 | 5.25 | 5.53 | 5.58 | 5.82 | 5.89[m] |
| $O_2$ (1/9) | 5.15 | 5.15 | 4.62 | 4.63 | 4.88 | 4.90 | 5.63 | 5.64[l] |
| OH (1/3) | 5.24 | 5.24 | 5.04 | 5.03 | 5.15 | 5.11 | 5.69 | |
| OH (1/9) | 4.93 | 4.93 | 4.40 | 4.42 | 4.71 | 4.92 | 5.39 | 4.93[d] |
| OOH (1/9) | 5.05 | 5.05 | 4.56 | 4.54 | 4.79 | 4.80 | 5.59 | |

[a]Sakong and Groß[120] AIMD (RPBE+D3), pH 0.1. [b]pH 7. [c]Vacuum. [d]$OH_{ads}$ at low coverage (1/12) at pH 7. [e]Bramley et al.[111] AIMD, (rVV10, CSHE). [f](PBE, CSHE). [g](rVV10, WF). [h](PBE, WF). [i]Le et al.[110] AIMD, PBE+D3. [j]Parker et al.[122] experimental O adsorption in UHV, low coverage. [k]High coverage. [l]Derry and Ross[121] experimental $O_2$ adsorption in UHV, low coverage. [m]High coverage.

At a surface charge density $\sigma = 0$, the calculated potential $U_{MIS}$(SHE) corresponds to the PZC of the system vs SHE. For the RISM (TIP5P) model at 1 M, we obtain a value of 0.39 V vs SHE, which is in good agreement with previous implicit solvation work: 0.54 V vs RHE[27] and 0.57 V vs SHE.[117] Moreover, our result is consistent with experimental values of 0.35 V vs RHE[118] and 0.37 V vs SHE.[119] In contrast, the SPC model yields an underestimated value of 0.10 V vs SHE, most likely due to the poor solvation energies for $H_3O^+$. The CANDLE model gives a higher value of 0.58 V, in good agreement with previous studies using implicit solvation models.

Finally, it is possible to link the calculated PZC values to the experimental scale by adding them to the IUPAC recommended value of 4.44 V,[104] resulting in solvated workfunctions that can be compared to experimental data. Table 3 compares the values obtained in this work with values from the theoretical and experimental literature. We note that our RISM (TIP5P) values for the clean Pt(111) surface are in good agreement with the study from Sakong and Groß,[120] where the authors performed AIMD using the same DFT functional and D3 dispersion correction (RPBE+D3). The model seems to follow the subtle trend of workfunction changes upon electrolyte concentration; our reported values of 4.97 and 4.81 eV for the clean Pt(111) surface are in close agreement with the value of 4.96 and 4.86 eV from the AIMD study. Additionally, our workfunction of 4.92 eV upon low coverage OH adsorption is also in good agreement with the value of 4.93 eV from the study. The CANDLE model shows similar trends, slightly overestimating the workfunctions giving 5.04 eV for the clean Pt(111) surface versus 4.86 eV from the AIMD study. Similarly, when OH is adsorbed, CANDLE predicts a value of 4.93 eV similar to the AIMD study.

Along with the RISM (SPC) model, the CANDLE model does not show significant variations in workfunction upon changes in electrolyte concentration. The workfunctions should highly depend on the orientation of water at the interface, which is heavily impacted by ionic adsorption on the surface. However, this explanation cannot be used for both RISM models since ions are not directly adsorbed on the surface (Supporting Information) but are located above the first water layers at the PZC and this behavior does not change with electrolyte concentration. For CANDLE, orientation is not accounted for, and we can conceptually understand the lack of variation. In this case, this also means that ionic concentration alone does not change the workfunction, or that the interface is already saturated at 0.1 M. For RISM models, the water density distributions (O($H_2O$) and H($H_2O$) sites in the Supporting Information) do not show significant variation with electrolyte concentration. However, the charge density plots for the TIP5P model show more important spatial differences as the concentration is changed from 0.1 to 1.0 M compared to the SPC model (Supporting Information). However, it is clear that such comparisons are far away from what is expected in a typical experimental electrochemical setup due to the absence of ionic adsorption. As a result these discussions are primarily confined to the context of RISM theory, and should be interpreted accordingly.

Nevertheless, the results obtained for all of our models are in good agreement with the literature. By performing AIMD and using the CSHE method, Bramley et al.[111] found values of 4.80 eV (rVV10) and 4.65 eV (PBE). When using the WF method, the authors found slightly higher values of 5.00 and 4.83 eV, further highlighting how the treatment of $\chi_S$ can affect the workfunctions. Similarly, Le et al.[110] reported a value of 4.7 eV for the workfunction at the solvated Pt(111) interface using AIMD with the PBE+D3 functional. Comparing these numbers and attempting to draw general conclusions, we see that CANDLE predicts slightly overestimated workfunctions, while RISM (SPC) underestimates them. RISM (TIP5P) seems to be the most reasonable model when compared with the literature. Table 3 shows a lowering of the workfunction upon solvation to be ≈0.6 eV for RISM (TIP5P), 0.5 eV for CANDLE, and 1.0 eV for RISM (SPC). Except for the latter, these values are far from the experimental expected decrease (≈−1.1 eV[110,123]). The underestimation of this effect by implicit solvation model is known[111] and is due to the misrepresentation of the polarization effects at the interface. The reasons are the lack of representation of water dipoles and the smoothed representation of polarization effects at the interface. Water dipole effects should be improved by RISM due to the spatial representation of (point)-charges. However, the lack of specific bonded interactions will lead to neglect of the polarization at the interface. Nevertheless, the three models perform relatively well considering that none of them were parametrized for this specific task. An additional point to consider is the initial underestimation of the vacuum workfunction by RPBE+D3,[120] giving 5.53 eV versus 5.9 eV from experimental measurements.[123,124] This is also reported by Sakong and Groß,[120] who found a value of 5.51 eV for the vacuum workfunction of Pt(111) (Table 3), leading to the underestimation of the solvated shift (−0.55 eV) in their AIMD study.



https://doi.org/10.1021/acs.jpcc.4c04924
J. Phys. Chem. C 2024, 128, 19586−19600

The literature on solvated workfunction values including explicit adsorbates is limited, and we were unable to find additional AIMD or experimental data to validate our findings. Nevertheless, the trends observed align with expected behavior, that is, an increase in workfunction upon surface oxidation. This pattern is well captured by the CANDLE solvation model, however, the RISM models generally exhibit more complex behaviors, deviating from the expected trend.

**Density Distributions.** In Figure 6 we compare the $O(H_2O)$ density profiles computed with the RISM models to

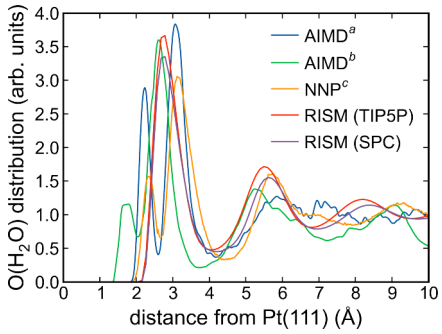


**Figure 6.** Comparison of $O(H_2O)$ density profiles calculated using the RISM models and AIMD data from various studies. Data were manually extracted in respective studies and normalized to their bulk densities. [a]Huang et al.[127] (AIMD, RPBE+D3); [b]Heenen et al.[28] (AIMD, RPBE+D3); [c]Mikkelsen et al.[125] (NNP, trained on PBE +D3).

AIMD data from various studies. The first striking discrepancy is the lack of double peak structure predicted by RISM vs explicit simulations. For both RISM models, the general picture is a representation of disorganized water layers with no clear separation between the first and second water layers. This hints at a representation of the water structure as a continuum of configurations between the two extreme cases, corresponding to a liquid-like water at the interface. This lack of a well-defined bilayer structure can be explained by considering the absence of specific adsorption in RISM versus explicit simulations where water molecules can weakly adsorb, explaining the low first peak of the water structure.[28,125,126]

The impact of the unit cell size and sampling on the persistence of the double peak structure in explicit simulations is unclear. AIMD studies often use small unit cells, which may lead to under- or overestimated bilayer structure due to enforced periodicity and restricted sampling. Heenen et al.[28] used a relatively small cell of 3 × 4 with 24 water molecules. In contrast, Huang et al.[127] employed a larger unit cell (6 × 6) containing 144 water molecules. Taking advantage of the reduced computational cost of their Neural Network Potential (NNP), Mikkelsen et al.[125] used a very large unit cell (33.2 Å × 38.6 Å) with 1024 water molecules. Their NNP was trained on smaller unit cells using the PBE+D3 functional. Despite the use of similar functionals and dispersion corrections in both AIMD studies, the agreement between results is poor, suggesting that the unit cell size and sampling have a significant impact. In our case, RISM gives a thermally integrated (fully sampled) picture of the interface, which might smooth out the double peak structure. However, given the overwhelming evidence of the double peak in AIMD studies, a more plausible explanation for the lack of this feature in our RISM simulations is the absence of bonding interactions.

Going beyond the double-peak considerations, both RISM models predict reasonable estimates of the distance between the water layer and the Pt(111) surface (≈ 2.8 Å). Similarly, the relative height of the peak with respect to the bulk concentration is reasonable. This is also true for the second smaller peak located further away from the surface, which is well reproduced by both RISM models.

The agreement in workfunction predictions between RISM and AIMD simulations, despite the failure to capture the characteristic double peak, is intriguing. The fine features of interfacial charge polarization, heavily influenced by water structure, are generally considered crucial for accurate workfunction predictions. The observed agreement might suggest that workfunctions are more sensitive to the average density distribution, which RISM adequately captures, rather than the fine details of water structure. Alternatively, this agreement could arise from a fortuitous cancellation of errors within the RISM framework.

To explore the effect of electronic charge, we performed calculations on clean and oxidized electrodes over a surface charge density range from −5 $\mu C/cm^2$ to +5 $\mu C/cm^2$, in increments of 1 $\mu C/cm^2$. This range was chosen by conducting prior calculations to determine the relevant potential range for the ORR, i.e., between 0.3 and 1.3 V. The water O-site and H-site density profile changes are presented in Figure 7.

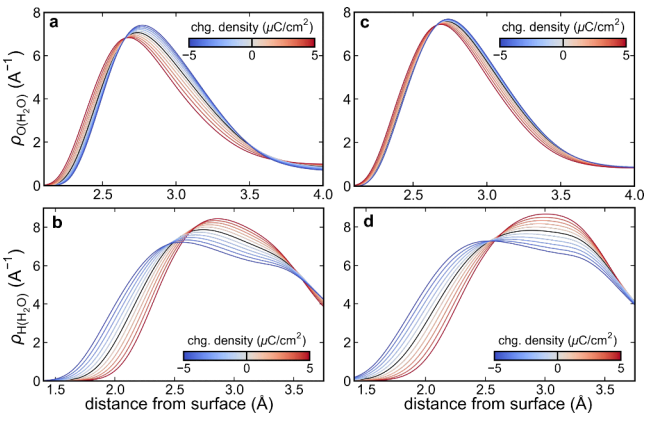


**Figure 7.** Pt(111) 3 × 3 density profile at varying surface charge densities for RISM $O(H_2O)$ and $H(H_2O)$ water sites along the direction perpendicular to the surface. Both (a, b) SPC and (c, d) TIP5P water models are shown with an electrolyte concentration of 0.1 M. The origin is chosen as the top layer of Pt atoms. The black line represents the density at the PZC.

For both models, the oxygen density maxima (Figures 7a and 7c) profile exhibit minimal variation versus surface charge density. This observation is consistent with the findings reported by Hinsch et al.[128] who noted that the distance between water molecules and the Pt(111) surface remained relatively constant across different applied potentials. In contrast, they found that the orientation of the water molecules, as indicated by the dipole orientation, varied significantly with the applied potential, with hydrogen atoms pointing away from the surface at positive potentials and toward the surface at negative potentials.

Nevertheless, both RISM (SPC) and RISM (TIP5P) models successfully reproduce the experimentally expected H-up to H-


https://doi.org/10.1021/acs.jpcc.4c04924
J. Phys. Chem. C 2024, 128, 19586−19600

down flip when crossing the PZC. This flip in the orientation of the water molecules at the interface is a key feature of the electrode−electrolyte interface and has been observed in various experimental and computational studies.[128−131] The ability of both models to capture this behavior is a testament to their accuracy in describing the basic electrostatic features of the electrochemical interface.

**Differential Capacitance.** Using the calculations performed at various surface charge densities in the previous section, it is possible to calculate capacitances by taking the linear slope of the charge vs potential curve (eq 13).

$$C_{\text{diff}} = \frac{d\sigma}{dU} = \frac{1}{2A}\frac{dq}{dU} \tag{13}$$

where $A$ is the surface area, $\sigma$ is the surface charge density, and $U$ is the potential. To obtain these capacitance curves from our discrete data we interpolate and employ numerical derivatives. Interpolations are done using Piecewise Cubic Hermite Interpolating Polynomials (PCHIP) to avoid any "overshoot" issues that can occur with classical cubic splines and to ensure the preservation of monotonicity.[132] Results are shown for the three models in Figure 8.

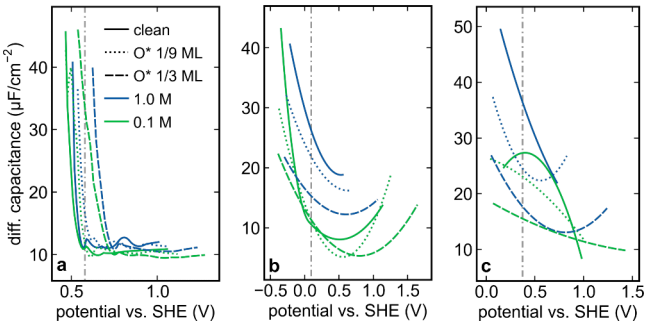


**Figure 8.** Differential capacitance versus potential curves obtained from the models (a) CANDLE, (b) RISM (SPC), and RISM (c) (TIP5P) at different electrolyte concentrations and oxygen coverages. Gray vertical lines are the PZCs predicted for the clean surface at 1.0 M.

For RISM models, we report Fermi energy fluctuations that can be close to 0.05 eV. Such small fluctuations do not change the conclusion for singular values, but derivatives will not be easily calculated without smoothing. For this reason, both Figures 8b and 8c have been fitted using a smoothing spline to allow observable trends. However, on a larger potential scale with larger steps, these fluctuations will be less impactful. Both RISM models give higher capacitances than the CANDLE model at the PZC, with 36 $\mu$F/cm$^2$ for RISM (TIP5P) and 25 $\mu$F/cm$^2$ for RISM (SPC) model. At high electrolyte concentration (1.0 M), higher capacitances are expected and are in good agreement with experimental studies.[119,133] At lower concentrations, the capacitance is expected to decrease and display a clear minimum at the PZC, ideally adopting a camel shaped curve. This behavior is not clearly observed for both of the RISM models, although a convex behavior can be recognized in some cases. This might be due to limitations of the current RISM models in accurately capturing the dielectric properties and short-range effects of the molecular solvent at the electrode−electrolyte interface. Recent work by Hagiwara et al.[134] has shown that the Dielectrically consistent Reference Interaction Site Model (DRISM), which introduces a correction term to couple solvent−solvent correlations with ion−solvent and ion−ion correlations, can lead to improved descriptions of the electrified interface. Further work will be needed to determine whether the DRISM model can provide a more accurate description of the capacitance behavior at the interface. The CANDLE model deviates from conventional linearized-Poisson−Boltzmann models, which often predict a near-constant capacitance vs potential behavior. Interestingly, the capacitance spike occurring at negative potentials was previously observed on other metallic systems[135] but described as unphysical.[136] This discrepancy suggests that the CANDLE model, despite its success in capturing some aspects of the electrode−electrolyte interface, may have limitations in accurately describing the capacitance behavior over a wide range of potentials.

Multiple experimental studies have shown the decrease of the double layer capacitance with oxygen coverage[137,138] on Pt(111), although this claim is not universal and should depend on the potential range and specific experimental conditions.[139] This behavior is correctly identified by both RISM models, which generally predict a decrease in capacitance with oxygen coverage. In contrast, oxidation does not seem to affect the capacitance in the CANDLE model.

## CONCLUSIONS

In this study, we investigated the applicability of the Reference Interaction Site Model (RISM) to the Pt(111) electrode, using two water parametrizations: 3-site (SPC) and 5-site (TIP5P). We compared our results with the CANDLE solvation model, which belongs to the class of nonlocal linearized Poisson−Boltzmann models. We used the ORR as a case study to assess the performance of the models for these catalytic reactions. Our results indicated that current RISM parametrizations do not enhance formation energies when compared to explicit water models. Both RISM water models predicted destabilization of the ORR intermediates, while explicit models suggested stabilization of most species. In contrast, the CANDLE model, in line with similar implicit models, predicted a small stabilization. This suggests room for improvement in the parametrization of O and H DFT solutes within the RISM framework, potentially leading to more accurate predictions of ORR intermediate formation energies.

We extensively discussed the differences between the models and attempted to explain the variation in solvation free energy with respect to the electrolyte concentration given by the RISM (TIP5P) model, which were not observed with the other models. To this end, we used 2D planar-averaged solvent charge distribution plots, which revealed that the description of the double layer differs significantly between the models. The TIP5P model showed a strong charge variation along the direction parallel to the electrode, in agreement with the CANDLE model. This was not observed in the SPC model, which displayed a simpler charge variation only along the direction perpendicular to the surface. From these discussions, it is clear that any arguments are self-consistent and should be interpreted in the context of RISM theory, with links to the experimental reality being speculative. Indeed, the lack of specific adsorption, especially of ions, greatly limits the comparison to experimental expectations.

After a comprehensive review of the various methods to compute workfunctions in solvent, we presented our (solvated) workfunctions for the clean Pt(111) surface and with explicit adsorbates. We found that the CANDLE model


https://doi.org/10.1021/acs.jpcc.4c04924
J. Phys. Chem. C 2024, 128, 19586−19600

was able to capture expected trends and provided reasonable results for the workfunction of the clean Pt(111) surface. Moreover, it predicted changes in workfunction upon explicit adsorption, as evidenced by comparison with results from an AIMD study. However, the model did not predict variation of workfunctions due to changes in electrolyte concentration. We found that the RISM (SPC) model underestimated the workfunction of the clean Pt(111) surface and failed to capture the expected trends due to explicit adsorbates and electrolyte concentration, predicting only minimal variations. Compared with the AIMD studies, the RISM (TIP5P) model was able to capture subtle effects due to electrolyte concentration and explicit adsorbates. With the evidence provided by the charge density plots, we deduced that the inclusion of lone pairs led to significant difference in the description of the electrochemical interface and were responsible for the accurate description of both solvation energies and workfunctions by the RISM (TIP5P) model, aligning well with previous studies which highlighted the important effect of lone-pairs on Pt(111).[110]

We continued the comparison of structural properties by investigating the thermally integrated $O(H_2O)$ density profile provided by both RISM models with the AIMD data. We found that both RISM models were unable to reproduce the expected double peak of oxygen distribution at the interface. The lack of this feature in RISM simulations is in agreement with the aforementioned absence of specific adsorption in the model. Despite this, both RISM models predicted a reasonable distance between the water layer and the Pt(111) surface, as well as the relative height of the peak with respect to the bulk concentration. Additionally, we studied the variation of these distributions upon surface charging by performing calculations at different surface charge densities. We found that the oxygen density profile remained relatively constant with charge variations, aligning with previous studies. However, the orientation of water molecules varied significantly with the applied potential, with hydrogen atoms pointing away from the surface at positive potentials and toward the surface at negative potentials. This key behavior was correctly captured by both RISM models, which predicted a H-down to H-up flip when crossing the PZC.

Finally, using the calculations performed outside the PZC, we calculated differential capacitance values for the three models on both the clean and oxidized surfaces. The higher capacitances predicted by the RISM models were consistent with experimental studies. Similarly, the decrease in capacitance due to oxygen coverage was correctly identified by both models. Nevertheless, we reported an important drawback in the RISM models with the presence of important Fermi energy fluctuations and computational instability that did not allow us to calculate differential capacitances accurately over the entire range of potentials.

Our results demonstrated that the RISM approach gives a comprehensive description of the complex interactions at the Pt(111) water interface with specific improvement compared to Poisson−Boltzmann models. The inclusion of lone-pairs in the TIP5P model proved to be a crucial factor in capturing the essential physics of the interface, including the correct description of solvation energies, workfunctions, and the double layer structure. These findings establish a foundation for comparing RISM with AIMD studies, opening avenues for further comparative studies, including the analysis of solvent densities and charge distributions around the electrode. Further improvements to the RISM parametrization of O and H DFT solutes and computational stability will be needed to move toward more accurate electrochemical simulations and to systematically incorporate RISM into computational studies.

## ■ ASSOCIATED CONTENT

### Supporting Information

The Supporting Information is available free of charge at https://pubs.acs.org/doi/10.1021/acs.jpcc.4c04924.

Comparison of vacuum results between JDFTx and Quantum Espresso; Additional details about phonon calculations and phonon density of states plots; Additional 2D-averaged charge and density plots for all models used in the main text (PDF)

## ■ AUTHOR INFORMATION


### Corresponding Author

**Chris-Kriton Skylaris** − *School of Chemistry, University of Southampton, Southampton SO17 1BJ, United Kingdom;* orcid.org/0000-0003-0258-3433; Email: C.Skylaris@soton.ac.uk

### Author

**Tom Demeyere** − *School of Chemistry, University of Southampton, Southampton SO17 1BJ, United Kingdom;* orcid.org/0000-0002-5023-6156

Complete contact information is available at: https://pubs.acs.org/10.1021/acs.jpcc.4c04924


### Notes

The authors declare no competing financial interest.

## ■ ACKNOWLEDGMENTS

The authors acknowledge the use of the IRIDIS 5 High Performance Computing Facility, and associated support services at the University of Southampton, in the completion of this work. We thank Dr. Gabriel Bramley, Emilie Gerouville, Maile Gerouville, and Davide Sarpa for proofreading. We also thank Prof. Minoru Otani, Prof. Philip Bartlett and Prof. Stephan Steinmann for their useful discussions. Finally, we thank Carole Demillecamps for her technical assistance in producing the figures presented in this work.

## ■ REFERENCES


(1) Stacy, J.; Regmi, Y. N.; Leonard, B.; Fan, M. The Recent Progress and Future of Oxygen Reduction Reaction Catalysis: A Review. *Renewable and Sustainable Energy Reviews* **2017**, *69*, 401−414.

(2) Kulkarni, A.; Siahrostami, S.; Patel, A.; Nørskov, J. K. Understanding Catalytic Activity Trends in the Oxygen Reduction Reaction. *Chem. Rev.* **2018**, *118*, 2302−2312.

(3) Shao, M.; Chang, Q.; Dodelet, J.-P.; Chenitz, R. Recent Advances in Electrocatalysts for Oxygen Reduction Reaction. *Chem. Rev.* **2016**, *116*, 3594−3657.

(4) Tian, F.; Anderson, A. B. Effective Reversible Potential, Energy Loss, and Overpotential on Platinum Fuel Cell Cathodes. *J. Phys. Chem. C* **2011**, *115*, 4076−4088.

(5) Gewirth, A. A.; Thorum, M. S. Electroreduction of Dioxygen for Fuel-Cell Applications: Materials and Challenges. *Inorg. Chem.* **2010**, *49*, 3557−3566.

(6) Zhang, J., Ed. *PEM Fuel Cell Electrocatalysts and Catalyst Layers: Fundamentals and Applications*; Springer: London, 2008.

(7) Brandon, N. P., Thompsett, D., Eds. *Fuel Cells Compendium*; Elsevier: Amsterdam, 2006.

(8) Acres, G. J. K.; Frost, J. C.; Hards, G. A.; Potter, R. J.; Ralph, T. R.; Thompsett, D.; Burstein, G. T.; Hutchings, G. J. Electrocatalysts for Fuel Cells. *Catal. Today* **1997**, *38*, 393−400.
(9) Fernandes, A. C.; Paganin, V. A.; Ticianelli, E. A. Degradation Study of Pt-based Alloy Catalysts for the Oxygen Reduction Reaction in Proton Exchange Membrane Fuel Cells. *J. Electroanal. Chem.* **2010**, *648*, 156−162.
(10) Nørskov, J. K.; Rossmeisl, J.; Logadottir, A.; Lindqvist, L.; Kitchin, J. R.; Bligaard, T.; Jónsson, H. Origin of the Overpotential for Oxygen Reduction at a Fuel-Cell Cathode. *J. Phys. Chem. B* **2004**, *108*, 17886−17892.
(11) Gasteiger, H. A.; Kocha, S. S.; Sompalli, B.; Wagner, F. T. Activity Benchmarks and Requirements for Pt, Pt-alloy, and Non-Pt Oxygen Reduction Catalysts for PEMFCs. *Appl. Catal. B: Environmental* **2005**, *56*, 9−35.
(12) Janik, M. J.; Taylor, C. D.; Neurock, M. First-Principles Analysis of the Initial Electroreduction Steps of Oxygen over Pt(111). *J. Electrochem. Soc.* **2009**, *156*, B126.
(13) Sui, S.; Wang, X.; Zhou, X.; Su, Y.; Riffat, S.; Liu, C.-j. A Comprehensive Review of Pt Electrocatalysts for the Oxygen Reduction Reaction: Nanostructure, Activity, Mechanism and Carbon Support in PEM Fuel Cells. *Journal of Materials Chemistry A* **2017**, *5*, 1808−1825.
(14) Huang, J.; Zhang, J.; Eikerling, M. Unifying Theoretical Framework for Deciphering the Oxygen Reduction Reaction on Platinum. *Phys. Chem. Chem. Phys.* **2018**, *20*, 11776−11786.
(15) Ikeshoji, T.; Otani, M. Toward Full Simulation of the Electrochemical Oxygen Reduction Reaction on Pt Using First-Principles and Kinetic Calculations. *Phys. Chem. Chem. Phys.* **2017**, *19*, 4447−4453.
(16) Keith, J. A.; Jerkiewicz, G.; Jacob, T. Theoretical Investigations of the Oxygen Reduction Reaction on Pt(111). *ChemPhysChem* **2010**, *11*, 2779−2794.
(17) Vinayan, B. P.; Nagar, R.; Ramaprabhu, S. Synthesis and Investigation of Mechanism of Platinum−Graphene Electrocatalysts by Novel Co-Reduction Techniques for Proton Exchange Membrane Fuel Cell Applications. *J. Mater. Chem.* **2012**, *22*, 25325−25334.
(18) Takagi, Y.; Wang, H.; Uemura, Y.; Nakamura, T.; Yu, L.; Sekizawa, O.; Uruga, T.; Tada, M.; Samjeské, G.; Iwasawa, Y.; et al. In Situ Study of Oxidation States of Platinum Nanoparticles on a Polymer Electrolyte Fuel Cell Electrode by near Ambient Pressure Hard X-ray Photoelectron Spectroscopy. *Phys. Chem. Chem. Phys.* **2017**, *19*, 6013−6021.
(19) Marenich, A. V.; Ho, J.; Coote, M. L.; Cramer, C. J.; Truhlar, D. G. Computational Electrochemistry: Prediction of Liquid-Phase Reduction Potentials. *Phys. Chem. Chem. Phys.* **2014**, *16*, 15068−15106.
(20) Sundararaman, R.; Goddard, W. A.; Arias, T. A. Grand Canonical Electronic Density-Functional Theory: Algorithms and Applications to Electrochemistry. *J. Chem. Phys.* **2017**, *146*, 114104.
(21) Alfonso, D.; Tafen, D.; Kauffmann, D. First-Principles Modeling in Heterogeneous Electrocatalysis. *Catalysts* **2018**, *8*, 424.
(22) Melander, M. M.; Kuisma, M. J.; Christensen, T. E. K.; Honkala, K. Grand-Canonical Approach to Density Functional Theory of Electrocatalytic Systems: Thermodynamics of Solid-Liquid Interfaces at Constant Ion and Electrode Potentials. *J. Chem. Phys.* **2019**, *150*, 041706.
(23) Bhandari, A.; Peng, C.; Dziedzic, J.; Anton, L.; Owen, J. R.; Kramer, D.; Skylaris, C.-K. Electrochemistry from First-Principles in the Grand Canonical Ensemble. *J. Chem. Phys.* **2021**, *155*, 024114.
(24) Bonnet, N.; Morishita, T.; Sugino, O.; Otani, M. First-Principles Molecular Dynamics at a Constant Electrode Potential. *Phys. Rev. Lett.* **2012**, *109*, 266101.
(25) Hagiwara, S.; Hu, C.; Nishihara, S.; Otani, M. Bias-Dependent Diffusion of a H 2 O Molecule on Metal Surfaces by the First-Principles Method under the Grand-Canonical Ensemble. *Phys. Rev. Mater.* **2021**, *5*, 065001.
(26) Pliego, J. R.; Riveros, J. M. Hybrid Discrete-continuum Solvation Methods. *WIREs Comput. Mol. Sci.* **2020**, *10*, No. e1440.
(27) Yeh, K.-Y.; Janik, M. J. Density Functional Theory-Based Electrochemical Models for the Oxygen Reduction Reaction: Comparison of Modeling Approaches for Electric Field and Solvent Effects. *J. Comput. Chem.* **2011**, *32*, 3399−3408.
(28) Heenen, H. H.; Gauthier, J. A.; Kristoffersen, H. H.; Ludwig, T.; Chan, K. Solvation at Metal/Water Interfaces: An *Ab Initio* Molecular Dynamics Benchmark of Common Computational Approaches. *J. Chem. Phys.* **2020**, *152*, 144703.
(29) Keilbart, N.; Okada, Y.; Feehan, A.; Higai, S.; Dabo, I. Quantum-Continuum Simulation of the Electrochemical Response of Pseudocapacitor Electrodes under Realistic Conditions. *Phys. Rev. B* **2017**, *95*, 115423.
(30) Weitzner, S. E.; Dabo, I. Voltage-Dependent Cluster Expansion for Electrified Solid-Liquid Interfaces: Application to the Electrochemical Deposition of Transition Metals. *Phys. Rev. B* **2017**, *96*, 205134.
(31) Tripković, V.; Skúlason, E.; Siahrostami, S.; Nørskov, J. K.; Rossmeisl, J. The Oxygen Reduction Reaction Mechanism on Pt(111) from Density Functional Theory Calculations. *Electrochim. Acta* **2010**, *55*, 7975−7981.
(32) Tripkovic, V.; Vegge, T. Potential- and Rate-Determining Step for Oxygen Reduction on Pt(111). *J. Phys. Chem. C* **2017**, *121*, 26785−26793.
(33) Rossmeisl, J.; Skúlason, E.; Björketun, M. E.; Tripkovic, V.; Nørskov, J. K. Modeling the Electrified Solid−Liquid Interface. *Chem. Phys. Lett.* **2008**, *466*, 68−71.
(34) Chan, K.; Nørskov, J. K. Electrochemical Barriers Made Simple. *J. Phys. Chem. Lett.* **2015**, *6*, 2663−2668.
(35) Liu, S.; White, M. G.; Liu, P. Mechanism of Oxygen Reduction Reaction on Pt(111) in Alkaline Solution: Importance of Chemisorbed Water on Surface. *J. Phys. Chem. C* **2016**, *120*, 15288−15298.
(36) Debye, P.; Hückel, E. De la theorie des electrolytes. I. abaissement du point de congelation et phenomenes associes. *Physikalische Zeitschrift* **1923**, *24*, 185−206.
(37) Bell, R. P. The Electrostatic Energy of Dipole Molecules in Different Media. *Trans. Faraday Soc.* **1931**, *27*, 797.
(38) Onsager, L. Electric Moments of Molecules in Liquids. *J. Am. Chem. Soc.* **1936**, *58*, 1486−1493.
(39) Miertuš, S.; Scrocco, E.; Tomasi, J. Electrostatic Interaction of a Solute with a Continuum. A Direct Utilizaion of AB Initio Molecular Potentials for the Prevision of Solvent Effects. *Chem. Phys.* **1981**, *55*, 117−129.
(40) Still, W. C.; Tempczyk, A.; Hawley, R. C.; Hendrickson, T. Semianalytical Treatment of Solvation for Molecular Mechanics and Dynamics. *J. Am. Chem. Soc.* **1990**, *112*, 6127−6129.
(41) Floris, F. M.; Tomasi, J.; Ahuir, J. L. P. Dispersion and Repulsion Contributions to the Solvation Energy: Refinements to a Simple Computational Model in the Continuum Approximation. *J. Comput. Chem.* **1991**, *12*, 784−791.
(42) Klamt, A.; Schüürmann, G. COSMO: A New Approach to Dielectric Screening in Solvents with Explicit Expressions for the Screening Energy and Its Gradient. *J. Chem. Soc., Perkin Trans.* **1993**, *2*, 799−805.
(43) Foresman, J. B.; Keith, T. A.; Wiberg, K. B.; Snoonian, J.; Frisch, M. J. Solvent Effects. 5. Influence of Cavity Shape, Truncation of Electrostatics, and Electron Correlation on Ab Initio Reaction Field Calculations. *J. Phys. Chem.* **1996**, *100*, 16098−16104.
(44) Cancès, E.; Mennucci, B.; Tomasi, J. A New Integral Equation Formalism for the Polarizable Continuum Model: Theoretical Background and Applications to Isotropic and Anisotropic Dielectrics. *J. Chem. Phys.* **1997**, *107*, 3032−3041.
(45) Fattebert, J.-L.; Gygi, F. Density Functional Theory for Efficientab Initio Molecular Dynamics Simulations in Solution. *J. Comput. Chem.* **2002**, *23*, 662−666.
(46) Ramirez, R.; Borgis, D. Density Functional Theory of Solvation and Its Relation to Implicit Solvent Models. *J. Phys. Chem. B* **2005**, *109*, 6754−6763.
(47) Tomasi, J.; Mennucci, B.; Cammi, R. Quantum Mechanical Continuum Solvation Models. *Chem. Rev.* **2005**, *105*, 2999−3094.

(48) Scherlis, D. A.; Fattebert, J.-L.; Gygi, F.; Cococcioni, M.; Marzari, N. A Unified Electrostatic and Cavitation Model for First-Principles Molecular Dynamics in Solution. *J. Chem. Phys.* **2006**, *124*, 074103.
(49) Ren, P.; Chun, J.; Thomas, D. G.; Schnieders, M. J.; Marucho, M.; Zhang, J.; Baker, N. A. Biomolecular Electrostatics and Solvation: A Computational Perspective. *Q. Rev. Biophys.* **2012**, *45*, 427−491.
(50) Skyner, R. E.; McDonagh, J. L.; Groom, C. R.; van Mourik, T.; Mitchell, J. B. O. A Review of Methods for the Calculation of Solution Free Energies and the Modelling of Systems in Solution. *Phys. Chem. Chem. Phys.* **2015**, *17*, 6174−6191.
(51) Sundararaman, R.; Schwarz, K. A.; Letchworth-Weaver, K.; Arias, T. A. Spicing up Continuum Solvation Models with SaLSA: The Spherically-Averaged Liquid Susceptibility Ansatz. *J. Chem. Phys.* **2015**, *142*, 054102.
(52) Hörmann, N. G.; Guo, Z.; Ambrosio, F.; Andreussi, O.; Pasquarello, A.; Marzari, N. Absolute Band Alignment at Semiconductor-Water Interfaces Using Explicit and Implicit Descriptions for Liquid Water. *npj Comput. Mater.* **2019**, *5*, 1−6.
(53) Kovalenko, A.; Hirata, F. Potentials of Mean Force of Simple Ions in Ambient Aqueous Solution. I. Three-dimensional Reference Interaction Site Model Approach. *J. Chem. Phys.* **2000**, *112*, 10391−10402.
(54) Kovalenko, A. Molecular Theory of Solvation: Methodology Summary and Illustrations. *Condensed Matter Physics* **2015**, *18*, 32601.
(55) Giannozzi, P.; Baroni, S.; Bonini, N.; Calandra, M.; Car, R.; Cavazzoni, C.; Ceresoli, D.; Chiarotti, G. L.; Cococcioni, M.; Dabo, I.; et al. QUANTUM ESPRESSO: A Modular and Open-Source Software Project for Quantum Simulations of Materials. *Journal of Physics. Condensed Matter: An Institute of Physics Journal* **2009**, *21*, 395502.
(56) Giannozzi, P.; Andreussi, O.; Brumme, T.; Bunau, O.; Nardelli, M. B.; Calandra, M.; Car, R.; Cavazzoni, C.; Ceresoli, D.; Cococcioni, M.; et al. Advanced Capabilities for Materials Modelling with Quantum ESPRESSO. *J. Phys.: Condens. Matter* **2017**, *29*, 465901.
(57) Weitzner, S. E.; Akhade, S. A.; Varley, J. B.; Wood, B. C.; Otani, M.; Baker, S. E.; Duoss, E. B. Toward Engineering of Solution Microenvironments for the CO2 Reduction Reaction: Unraveling pH and Voltage Effects from a Combined Density-Functional−Continuum Theory. *J. Phys. Chem. Lett.* **2020**, *11*, 4113−4118.
(58) Tesch, R.; Kowalski, P. M.; Eikerling, M. H. Properties of the Pt(111)/Electrolyte Electrochemical Interface Studied with a Hybrid DFT−Solvation Approach. *J. Phys.: Condens. Matter* **2021**, *33*, 444004.
(59) Haruyama, J.; Ikeshoji, T.; Otani, M. Analysis of Lithium Insertion/Desorption Reaction at Interfaces between Graphite Electrodes and Electrolyte Solution Using Density Functional + Implicit Solvation Theory. *J. Phys. Chem. C* **2018**, *122*, 9804−9810.
(60) Nishihara, S.; Otani, M. Hybrid Solvation Models for Bulk, Interface, and Membrane: Reference Interaction Site Methods Coupled with Density Functional Theory. *Phys. Rev. B* **2017**, *96*, 115429.
(61) Otani, M.; Sugino, O. First-Principles Calculations of Charged Surfaces and Interfaces: A Plane-Wave Nonrepeated Slab Approach. *Phys. Rev. B* **2006**, *73*, 115407.
(62) Hamada, I.; Sugino, O.; Bonnet, N.; Otani, M. Improved Modeling of Electrified Interfaces Using the Effective Screening Medium Method. *Phys. Rev. B* **2013**, *88*, 155427.
(63) Fernandez-Alvarez, V. M.; Eikerling, M. H. Interface Properties of the Partially Oxidized Pt(111) Surface Using Hybrid DFT−Solvation Models. *ACS Appl. Mater. Interfaces* **2019**, *11*, 43774−43780.
(64) Berendsen, H. J. C.; Postma, J. P. M.; van Gunsteren, W. F.; Hermans, J. In *Intermolecular Forces: Proceedings of the Fourteenth Jerusalem Symposium on Quantum Chemistry and Biochemistry Held in Jerusalem, Israel, April 13−16, 1981*; Pullman, B., Ed.; Springer Netherlands: Dordrecht, 1981; pp 331−342.
(65) Mahoney, M. W.; Jorgensen, W. L. A Five-Site Model for Liquid Water and the Reproduction of the Density Anomaly by Rigid, Nonpolarizable Potential Functions. *J. Chem. Phys.* **2000**, *112*, 8910−8922.
(66) Sundararaman, R.; Goddard, W. A. The Charge-Asymmetric Nonlocally Determined Local-Electric (CANDLE) Solvation Model. *J. Chem. Phys.* **2015**, *142*, 064107.
(67) Lejaeghere, K.; Bihlmayer, G.; Björkman, T.; Blaha, P.; Blügel, S.; Blum, V.; Caliste, D.; Castelli, I. E.; Clark, S. J.; Dal Corso, A.; et al. Reproducibility in Density Functional Theory Calculations of Solids. *Science* **2016**, *351*, aad3000.
(68) Dal Corso, A. Pseudopotentials Periodic Table: From H to Pu. *Comput. Mater. Sci.* **2014**, *95*, 337−350.
(69) Kucukbenli, E.; Monni, M.; Adetunji, B. I.; Ge, X.; Adebayo, G. A.; Marzari, N.; de Gironcoli, S.; Corso, A. D. Projector Augmented-Wave and All-Electron Calculations across the Periodic Table: A Comparison of Structural and Energetic Properties. *arXiv*, April 11, 2014. DOI: 10.48550/arXiv.1404.3015.
(70) Hamann, D. R. Optimized Norm-Conserving Vanderbilt Pseudopotentials. *Phys. Rev. B* **2013**, *88*, 085117.
(71) Monkhorst, H. J.; Pack, J. D. Special Points for Brillouin-zone Integrations. *Phys. Rev. B* **1976**, *13*, 5188−5192.
(72) Hammer, B.; Hansen, L. B.; Nørskov, J. K. Improved Adsorption Energetics within Density-Functional Theory Using Revised Perdew-Burke-Ernzerhof Functionals. *Phys. Rev. B* **1999**, *59*, 7413−7421.
(73) Grimme, S.; Antony, J.; Ehrlich, S.; Krieg, H. A Consistent and Accurate Ab Initio Parametrization of Density Functional Dispersion Correction (DFT-D) for the 94 Elements H-Pu. *J. Chem. Phys.* **2010**, *132*, 154104.
(74) Sakong, S.; Naderian, M.; Mathew, K.; Hennig, R. G.; Groß, A. Density Functional Theory Study of the Electrochemical Interface between a Pt Electrode and an Aqueous Electrolyte Using an Implicit Solvent Method. *J. Chem. Phys.* **2015**, *142*, 234107.
(75) Haruyama, J.; Ikeshoji, T.; Otani, M. Electrode Potential from Density Functional Theory Calculations Combined with Implicit Solvation Theory. *Phys. Rev. Mater.* **2018**, *2*, 095801.
(76) Kano, K.; Hagiwara, S.; Igarashi, T.; Otani, M. Study on the Free Corrosion Potential at an Interface between an Al Electrode and an Acidic Aqueous NaCl Solution through Density Functional Theory Combined with the Reference Interaction Site Model. *Electrochim. Acta* **2021**, *377*, 138121.
(77) Chuev, G. N.; Chiodo, S.; Erofeeva, S. E.; Fedorov, M. V.; Russo, N.; Sicilia, E. A Quasilinear RISM Approach for the Computation of Solvation Free Energy of Ionic Species. *Chem. Phys. Lett.* **2006**, *418*, 485−489.
(78) Smith, D. E.; Dang, L. X. Computer Simulations of NaCl Association in Polarizable Water. *J. Chem. Phys.* **1994**, *100*, 3757−3766.
(79) Sundararaman, R.; Letchworth-Weaver, K.; Schwarz, K. A.; Gunceler, D.; Ozhabes, Y.; Arias, T. A. JDFTx: Software for Joint Density-Functional Theory. *SoftwareX* **2017**, *6*, 278−284.
(80) Vasić, D.; Pašti, I.; Gavrilov, N.; Mentus, S. DFT Study of Interaction of O, O2, and OH with Unreconstructed Pt(Hkl) (h, k, l = 0, 1) Surfaces—Similarities, Differences, and Universalities. *Russian Journal of Physical Chemistry A* **2013**, *87*, 2214−2218.
(81) Jinnouchi, R.; Kodama, K.; Morimoto, Y. DFT Calculations on H, OH and O Adsorbate Formations on Pt(111) and Pt(332) Electrodes. *J. Electroanal. Chem.* **2014**, *716*, 31−44.
(82) Sha, Y.; Yu, T. H.; Liu, Y.; Merinov, B. V.; Goddard, W. A. Theoretical Study of Solvent Effects on the Platinum-Catalyzed Oxygen Reduction Reaction. *J. Phys. Chem. Lett.* **2010**, *1*, 856−861.
(83) Iyemperumal, S. K.; Deskins, N. A. Evaluating Solvent Effects at the Aqueous/Pt(111) Interface. *ChemPhysChem* **2017**, *18*, 2171−2190.
(84) Gray, C. M.; Saravanan, K.; Wang, G.; Keith, J. A. Quantifying Solvation Energies at Solid/Liquid Interfaces Using Continuum Solvation Methods. *Mol. Simul.* **2017**, *43*, 420−427.
(85) Zhang, Q.; Asthagiri, A. Solvation Effects on DFT Predictions of ORR Activity on Metal Surfaces. *Catal. Today* **2019**, *323*, 35−43.

(86) Calle-Vallejo, F.; de Morais, R. F.; Illas, F.; Loffreda, D.; Sautet, P. Affordable Estimation of Solvation Contributions to the Adsorption Energies of Oxygenates on Metal Nanoparticles. *J. Phys. Chem. C* **2019**, *123*, 5578−5582.
(87) Abidin, A. F. Z.; Hamada, I. Oxygen Reduction Reaction on Single-Atom Catalysts From Density Functional Theory Calculations Combined with an Implicit Solvation Model. *J. Phys. Chem. C* **2023**, *127*, 13623−13631.
(88) Kirchhoff, B.; Jónsson, E. Ö.; Jacob, T.; Jónsson, H. On the Challenge of Obtaining an Accurate Solvation Energy Estimate in Simulations of Electrocatalysis. *Top. Catal.* **2023**, *66*, 1244−1259.
(89) Yeh, K.-Y.; Wasileski, S. A.; Janik, M. J. Electronic Structure Models of Oxygen Adsorption at the Solvated, Electrified Pt(111) Interface. *Phys. Chem. Chem. Phys.* **2009**, *11*, 10108.
(90) Chun, H.-J.; Morankar, A.; Zeng, Z.; Greeley, J. Solvation Enthalpy Determination for Aqueous-Phase Reaction Adsorbates Using Ab Initio Molecular Dynamics-Based Structure Sampling. *J. Phys. Chem. C* **2024**, *128*, 1621−1632.
(91) Kronberg, R. *Ab Initio Molecular Dynamics Simulation of the Platinum−Water Interface: Insights into Structure and Electrocatalytic Properties*. Ph.D. thesis, 2018.
(92) Nair, A. S.; Pathak, B. Accounting for Dispersion Effects in the DFT Framework of Electrocatalysis: A Hybrid Solvation Model-Based Case Study of the Oxygen Reduction Reaction. *J. Phys. Chem. C* **2022**, *126*, 6171−6188.
(93) Linstrom, P. *NIST Chemistry WebBook*; NIST Standard Reference Database 69. 1997.
(94) Bramley, G. A.; Nguyen, M.-T.; Glezakou, V.-A.; Rousseau, R.; Skylaris, C.-K. Understanding Adsorption of Organics on Pt(111) in the Aqueous Phase: Insights from DFT Based Implicit Solvent and Statistical Thermodynamics Models. *J. Chem. Theory Comput.* **2022**, *18*, 1849.
(95) Gim, S.; Cho, K. J.; Lim, H.-K.; Kim, H. Structure, Dynamics, and Wettability of Water at Metal Interfaces. *Sci. Rep.* **2019**, *9*, 14805.
(96) Sakong, S.; Groß, A. Water Structures on a Pt(111) Electrode from Ab Initio Molecular Dynamic Simulations for a Variety of Electrochemical Conditions. *Phys. Chem. Chem. Phys.* **2020**, *22*, 10431−10437.
(97) Campbell, C. T.; Sellers, J. R. V. The Entropies of Adsorbed Molecules. *J. Am. Chem. Soc.* **2012**, *134*, 18109−18115.
(98) He, Z.-D.; Hanselman, S.; Chen, Y.-X.; Koper, M. T. M.; Calle-Vallejo, F. Importance of Solvation for the Accurate Prediction of Oxygen Reduction Activities of Pt-Based Electrocatalysts. *J. Phys. Chem. Lett.* **2017**, *8*, 2243−2246.
(99) Di Liberto, G.; Giordano, L. Role of Solvation Model on the Stability of Oxygenates on Pt(111): A Comparison between Microsolvation, Extended Bilayer, and Extended Metal/Water Interface. *Electrochem. Sci. Adv.* **2024**, *4*, No. e2100204.
(100) Lee, K.; Schmidt, J. R. Correcting Implicit Solvation at Metal/Water Interfaces through the Incorporation of Competitive Water Adsorption. *J. Chem. Phys.* **2024**, *161*, 041103.
(101) Rumptz, J. R.; Campbell, C. T. Adhesion Energies of Solvent Films to Pt(111) and Ni(111) Surfaces by Adsorption Calorimetry. *ACS Catal.* **2019**, *9*, 11819−11825.
(102) Cheng, J.; Sprik, M. Alignment of Electronic Energy Levels at Electrochemical Interfaces. *Phys. Chem. Chem. Phys.* **2012**, *14*, 11245.
(103) Fawcett, W. R. The Ionic Work Function and Its Role in Estimating Absolute Electrode Potentials. *Langmuir* **2008**, *24*, 9868−9875.
(104) Trasatti, S. The Absolute Electrode Potential: An Explanatory Note (Recommendations 1986). *Pure Appl. Chem.* **1986**, *58*, 955−966.
(105) Togo, A. First-Principles Phonon Calculations with Phonopy and Phono3py. *J. Phys. Soc. Jpn.* **2023**, *92*, 012001.
(106) Togo, A.; Chaput, L.; Tadano, T.; Tanaka, I. Implementation Strategies in Phonopy and Phono3py. *J. Phys.: Condens. Matter* **2023**, *35*, 353001.
(107) Chase, M. W. *NIST-JANAF Thermochemical Tables*, 4th ed.; NIST, 1998.
(108) Palascak, M. W.; Shields, G. C. Accurate Experimental Values for the Free Energies of Hydration of H+, OH-, and H3O+. *J. Phys. Chem. A* **2004**, *108*, 3692−3694.
(109) Butin, O.; Pereyaslavets, L.; Kamath, G.; Illarionov, A.; Sakipov, S.; Kurnikov, I. V.; Voronina, E.; Ivahnenko, I.; Leontyev, I.; Nawrocki, G.; et al. The Determination of Free Energy of Hydration of Water Ions from First Principles. *J. Chem. Theory Comput.* **2024**, *20*, 5215−5224.
(110) Le, J.; Iannuzzi, M.; Cuesta, A.; Cheng, J. Determining Potentials of Zero Charge of Metal Electrodes versus the Standard Hydrogen Electrode from Density-Functional-Theory-Based Molecular Dynamics. *Phys. Rev. Lett.* **2017**, *119*, 016801.
(111) Bramley, G.; Nguyen, M.-T.; Glezakou, V.-A.; Rousseau, R.; Skylaris, C.-K. Reconciling Work Functions and Adsorption Enthalpies for Implicit Solvent Models: A Pt (111)/Water Interface Case Study. *J. Chem. Theory Comput.* **2020**, *16*, 2703−2715.
(112) Trasatti, S. Interfacial Behaviour of Non-Aqueous Solvents. *Electrochim. Acta* **1987**, *32*, 843−850.
(113) Krishtalik, L. I. The Surface Potential of Solvent and the Intraphase Pre-Existing Potential. *Russian Journal of Electrochemistry* **2008**, *44*, 43−49.
(114) Lamoureux, G.; Roux, B. Absolute Hydration Free Energy Scale for Alkali and Halide Ions Established from Simulations with a Polarizable Force Field. *J. Phys. Chem. B* **2006**, *110*, 3308−3322.
(115) Mathew, K.; Kolluru, V. S. C.; Mula, S.; Steinmann, S. N.; Hennig, R. G. Implicit Self-Consistent Electrolyte Model in Plane-Wave Density-Functional Theory. *J. Chem. Phys.* **2019**, *151*, 234101.
(116) Gunceler, D.; Letchworth-Weaver, K.; Sundararaman, R.; Schwarz, K. A.; Arias, T. A. The Importance of Nonlinear Fluid Response in Joint Density-Functional Theory Studies of Battery Systems. *Modell. Simul. Mater. Sci. Eng.* **2013**, *21*, 074005.
(117) Hörmann, N. G.; Andreussi, O.; Marzari, N. Grand Canonical Simulations of Electrochemical Interfaces in Implicit Solvation Models. *J. Chem. Phys.* **2019**, *150*, 041730.
(118) Iwasita, T.; Nart, F. C. In Situ Infrared Spectroscopy at Electrochemical Interfaces. *Prog. Surf. Sci.* **1997**, *55*, 271−340.
(119) Pajkossy, T.; Kolb, D. M. Double Layer Capacitance of Pt(111) Single Crystal Electrodes. *Electrochim. Acta* **2001**, *46*, 3063−3071.
(120) Sakong, S.; Groß, A. The Electric Double Layer at Metal-Water Interfaces Revisited Based on a Charge Polarization Scheme. *J. Chem. Phys.* **2018**, *149*, 084705.
(121) Derry, G. N.; Ross, P. N. A Work Function Change Study of Oxygen Adsorption on Pt(111) and Pt(100). *J. Chem. Phys.* **1985**, *82*, 2772−2778.
(122) Parker, D. H.; Bartram, M. E.; Koel, B. E. Study of High Coverages of Atomic Oxygen on the Pt(111) Surface. *Surf. Sci.* **1989**, *217*, 489−510.
(123) Ranke, W. Low Temperature Adsorption and Condensation of O2, H2O and NO on Pt(111), Studied by Core Level and Valence Band Photoemission. *Surf. Sci.* **1989**, *209*, 57−76.
(124) Kiskinova, M.; Pirug, G.; Bonzel, H. Adsorption and Decomposition of H2O on a K-covered Pt(111) Surface. *Surf. Sci.* **1985**, *150*, 319−338.
(125) Mikkelsen, A. E. G.; Schiøtz, J.; Vegge, T.; Jacobsen, K. W. Is the Water/Pt(111) Interface Ordered at Room Temperature? *J. Chem. Phys.* **2021**, *155*, 224701.
(126) Groß, A.; Sakong, S. Ab Initio Simulations of Water/Metal Interfaces. *Chem. Rev.* **2022**, *122*, 10746−10776.
(127) Huang, J.; Zhang, Y.; Li, M.; Groß, A.; Sakong, S. Comparing Ab Initio Molecular Dynamics and a Semiclassical Grand Canonical Scheme for the Electric Double Layer of the Pt(111)/Water Interface. *J. Phys. Chem. Lett.* **2023**, *14*, 2354−2363.
(128) Hinsch, J. J.; Bouzid, A.; Barker, J. C.; White, J. J.; Mortier, F.; Zhao, H.; Wang, Y. Revisiting the Electrified Pt(111)/Water Interfaces through an Affordable Double-Reference Ab Initio Approach. *J. Phys. Chem. C* **2023**, *127*, 19857−19866.

(129) Habib, M. A.; Bockris, J. O. Potential-Dependent Water Orientation: An in Situ Spectroscopic Study. *Langmuir* **1986**, *2*, 388−392.
(130) Osawa, M.; Tsushima, M.; Mogami, H.; Samjeské, G.; Yamakata, A. Structure of Water at the Electrified Platinum-Water Interface: A Study by Surface-Enhanced Infrared Absorption Spectroscopy. *J. Phys. Chem. C* **2008**, *112*, 4248−4256.
(131) Wiebe, J.; Spohr, E. Water Structure and Mechanisms of Proton Discharge on Platinum Electrodes: Empirical Valence Bond Molecular Dynamics Trajectory Studies. *Electrocatalysis* **2017**, *8*, 637−646.
(132) Fritsch, F. N.; Carlson, R. E. Monotone Piecewise Cubic Interpolation. *SIAM Journal on Numerical Analysis* **1980**, *17*, 238−246.
(133) May, S. Differential Capacitance of the Electric Double Layer: Mean-Field Modeling Approaches. *Current Opinion in Electrochemistry* **2019**, *13*, 125−131.
(134) Hagiwara, S.; Nishihara, S.; Kuroda, F.; Otani, M. Development of a Dielectrically Consistent Reference Interaction Site Model Combined with the Density Functional Theory for Electrochemical Interface Simulations. *Phys. Rev. Mater.* **2022**, *6*, 093802.
(135) Sundararaman, R.; Schwarz, K. Evaluating Continuum Solvation Models for the Electrode-Electrolyte Interface: Challenges and Strategies for Improvement. *J. Chem. Phys.* **2017**, *146*, 084111.
(136) Sundararaman, R.; Letchworth-Weaver, K.; Schwarz, K. A. Improving Accuracy of Electrochemical Capacitance and Solvation Energetics in First-Principles Calculations. *J. Chem. Phys.* **2018**, *148*, 144105.
(137) Gilman, S. Electrochemical Surface Oxidation of Platinum. *Electrochim. Acta* **1964**, *9*, 1025−1046.
(138) Pell, W. G.; Zolfaghari, A.; Conway, B. E. Capacitance of the Double-Layer at Polycrystalline Pt Electrodes Bearing a Surface-Oxide Film. *J. Electroanal. Chem.* **2002**, *532*, 13−23.
(139) Rosen, M.; Flinn, D. R.; Schuldiner, S. Double Layer Capacitance on Platinum in 1M H$_2$SO$_4$ from the Reversible Hydrogen Potential to the Oxygen Formation Region. *J. Electrochem. Soc.* **1969**, *116*, 1112.


https://doi.org/10.1021/acs.jpcc.4c04924
*J. Phys. Chem. C* 2024, 128, 19586−19600